

See discussions, stats, and author profiles for this publication at: <https://www.researchgate.net/publication/259884803>

Role of Solvent and External Growth Environments to Determine Growth Morphology of Molecular Crystals

ARTICLE in CRYSTAL GROWTH & DESIGN · JUNE 2013

Impact Factor: 4.89 · DOI: 10.1021/cg4005196

CITATIONS

15

READS

43

2 AUTHORS:



Manoj Kumar Singh

Raja Ramanna Centre for Advanced Technology

18 PUBLICATIONS 96 CITATIONS

[SEE PROFILE](#)



Arup Banerjee

Raja Ramanna Centre for Advanced Technology

79 PUBLICATIONS 693 CITATIONS

[SEE PROFILE](#)

Role of Solvent and External Growth Environments to Determine Growth Morphology of Molecular Crystals

M. K. Singh*,† and Arup Banerjee‡,§

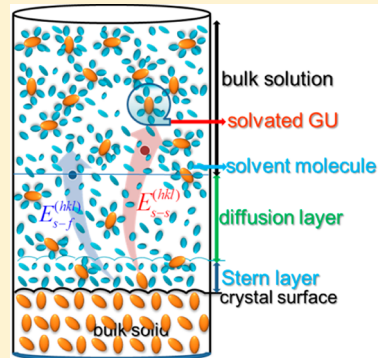
†Laser Materials Development and Devices Division, Raja Ramanna Centre for Advanced Technology, Indore, India

‡BARC Training School at RRCAT, Raja Ramanna Centre for Advanced Technology, Indore, India

§Homi Bhabha National Institute, Department of Atomic Energy, Indore, India

Supporting Information

ABSTRACT: We report a computational method to investigate the mechanism through which the solvent interacts with the crystal surfaces during the crystal growth process. We have considered the role of the internal, crystal-solution interfacial structure and external growth environments affecting crystal growth to predict the growth morphology by calculating relative growth rate of different crystal faces. The interfacial structure and bonding energies of solute and solvent molecules of faces having different crystallographic orientations are obtained using periodic first-principles density functional method. The effects of molecular orientation of growth units and surface relaxation of the habit faces have also been considered in order to identify the adsorption of rate-determining molecules to different faces of crystals for their growth. On the basis of the analysis of interfacial structure and external growth environment, the expression for growth rates relating the level of supersaturation, temperature, solubility, bonding energies of solute–surface, solvent–surface, and the rate of growth has been derived. The method is applied to study growth morphology of two molecular crystals, namely, urea and β -succinic acid crystals from vapor and different solvents. The results obtained from calculations match well with the corresponding available experimental data. The remarkable agreement between the predicted growth shapes and the corresponding experimental results allow us to understand the role played by solvents and external growth factors on growth morphologies of molecular crystals.



1. INTRODUCTION

The structure of the crystal–solution interface determines many important physical and chemical processes which occur at the interface, such as crystal growth, wetting, lubrication, and catalysis.¹ The crystal surface (hereafter referred to as surface) at the interface can differ from the bulk-terminated crystallographic structure. It depends upon surface termination, the possible reconstruction and relaxation of the surface. Similarly, the atomic structure of liquid near the surface may differ from the liquid structure in the bulk because it experiences periodic potential at the surface, and it is expected to show more ordering than in a bulk liquid. The mechanism of action by which the crystal–solution interface exerts its influence is still a matter of debate. There are two distinct hypotheses that attempt to model the effect of solvent ordering in the interfacial region on crystal growth. In the surface roughening hypothesis,^{2–5} the favorable interaction of the solvent with specific crystal faces results in the reduction of the interfacial surface tension. The consequence is a transition from a smooth to a rough interface and a resultant increase in the rate of growth of the affected faces, and they become morphologically less important. Bourne et al.² have explained the growth of paraffin from light petroleum solutions⁶ and sucrose from aqueous solutions,⁷ using the surface-roughening hypothesis. In accordance with the second hypothesis, which is commonly known as the inhibition model, the solvent molecules exert

their effect by preferential adsorption upon the growing surfaces and inhibit the growth of specific faces^{8–11} since the solute molecules would be in competition with the solvent molecules for the growth sites. Thus, the highly ordered solvent molecules at the surfaces are expected to slow down the incorporation and diffusion of solute molecules. The incorporation of solute molecules to crystal faces would require removal of the periodically adsorbed solvent molecules from the surfaces. The inhibition model is consistent with the mechanism of action of tailor-made additives,^{8,12} which has a structure very similar to that of the molecule to be crystallized but for an altered moiety.¹³ Experimentally observed growth of *N*-n-octyl-D-gluconamide in methanol solution¹⁴ is explained through the inhibition model. On the other hand, the experimental growth rate measurement of the polar faces of (R, S)-alanine and γ -glycine crystals can only be explained by a complex, relay-type mechanism that does not fall in the realm of either of the two models.¹³ However, recent experimental growth rate measurement of the polar faces of DL-alanine crystal at high supersaturation shows the inability of the relay-type mechanism to explain the experimental observations.¹⁵

Received: January 22, 2013

Revised: May 16, 2013



The interfacial structure plays a very important role during the crystal growth process. In many cases, little is known about the molecular-scale structure of such interfacial layers, and therefore, the correlation between macroscopic phenomena and molecular-scale processes at the interface often remains speculative. In most of the cases, difficulty arises because of the fact that growth processes taking place at the molecular scale are barely or not at all accessible to experimental methods. Due to the advent of the intense X-ray beams provided by synchrotron radiation sources, surface X-ray diffraction is usually used to determine the structures of crystal surfaces and solid–liquid interfaces, which provide important insight into the liquid ordering on the crystal surfaces. To investigate the role of the interfacial structure in the actual growth process, it is necessary to have a detailed understanding of the interface.^{2,16}

It is well-established that the solvent along with other external growth factors like supersaturation, temperature, and solubility play a vital role in the determination of the crystal growth morphology, and thus by controlling these factors, crystal growers can engineer the shape of crystals in a desired manner. Predicting the growth shape also provides an important step in controlling the process parameters in the chemical and pharmaceutical industries. However, predicting the crystal morphology, taking into account the effects of solvents, solubility, temperature, and impurities, is still a formidable task. Recently, much attention has been paid to include the effects of solvent and supersaturation on crystal morphology. Liu et al.¹⁷ formulated a model based on the interfacial structure analysis and predicted the growth shape of urea crystals in aqueous solutions. They have carried out molecular dynamic simulations to produce the genuine interfacial structure in different crystallographic orientations. Gnanasambandam and Rajagopalan¹⁸ extended the idea of Liu et al.,¹⁷ what is known as extended interfacial structure analysis, to predict the shape of α -glycine crystals from aqueous solutions by fully accounting for the effects of the solvent. On the other hand, the computational approach developed by Doherty et al.¹⁹ is based on detailed analysis of the Burton–Cabrera–Frank (BCF) spiral growth mechanism,²⁰ augmented by additional terms, to account for the adhesion surface energy of the solvent at the interface. Piana et al.²¹ have utilized multiscale modeling to study the effect of solvent, supersaturation, and extended defects on the growth shape of the urea crystal from aqueous and methanol solutions.

In this paper, we have investigated the growth morphology of two molecular crystals, namely, urea and β -succinic acid crystals from vapor and solutions by calculating the relative growth rate of the morphologically important faces of these crystals. For this purpose, we have derived a growth rate expression which incorporates many internal and external growth parameters like molecular orientation of growth units (GUs), surface relaxation, interplanar distance, coordination number, supersaturation, solubility, temperature, and energetics for solute–surface and solvent–surface interactions to compute growth morphology. The habit of the urea crystal is known to change from blocklike to needlelike with a large aspect ratio (AS) when the crystal is grown from an aqueous/methanol solution than that from the vapor phase.²² Also, the growth rate and AS of the urea crystal obtained from the aqueous solution are higher than those from methanol solution.²³ The solvent-induced habit modification of β -succinic acid crystals has already been studied by several authors,^{24–31} but it is still not clear how solvent determines the

growth morphology. It is well-known that factors such as solvents and additives can affect the crystallization of β -succinic acid from solutions and result in different growth morphologies, by controlling the conditions of crystallization. The growth shapes of β -succinic acid crystals are known to change from a platelike habit with a dominant basal plane to a needlelike habit when water is replaced by isopropyl alcohol.²⁸ In this paper, we also investigate the effects of water and isopropyl alcohol on crystallization of the β -succinic acid crystal.

The relationship between the solvent interaction with different crystal faces and the resulting growth morphology is the focus of the present work. For this purpose, we employ the inhibition model in which interaction of solvent with the surface impedes the growth rate. We have extended the idea of the effective growth unit proposed by Liu et al.¹⁷ to calculate molecular attachment energies. Recently, we have also studied the role of molecular orientation to predict the growth shape of molecular crystals.^{32a} Our study showed that, in the case of a unit cell comprising more than one GU, the incorporation of the molecular orientation and surface relaxation to the attachment energy of GU can significantly enhance the predictive power of HP model.³³ Compared to the other approaches^{17,19,21} devoted to the prediction of crystal morphology from solution, our approach incorporates several internal and external growth parameters and the energetics characterizing solute–surface and solvent–surface interactions have been obtained using accurate dispersion-corrected density functional theory. The results obtained by us in this paper yield a detailed picture of the energetics of solute and solvent interactions at the crystal surfaces, and the growth morphologies predicted for the above-mentioned molecular crystals are in good agreement with the corresponding experimental results.

The rest of the paper is organized as follows. In Theoretical Methodology, we outline the theoretical formalism for the derivation of growth rate expression followed by a discussion on the computational method in Computational Details. The results obtained from our calculations are discussed and compared with the corresponding experimental morphologies of urea and succinic acid crystals in the Results and Discussion, and the paper is concluded in Conclusions.

2. THEORETICAL METHODOLOGY

We next present a detailed derivation of the rate of growth of faces, which enable us to study the effect of interfacial structure and external growth factors such as solvents, supersaturation, and temperature. It has been shown that monomers or dimers of the molecule are adsorbed during the growth of the ZnCd(SCN)₄ crystal.³⁴ Motivated by this study, we present a molecular scale model based on inhibition mechanism to determine crystal morphology (see Figure 1 of the Supporting Information). Accordingly, the crystal growth occurs due to the adsorption of GUs from the solution rather than the attachment of a slice of one d_{hkl} thickness upon the crystal surfaces. The GUs can be described as the smallest cluster (a molecule, complexes, or ions) occurring in solution and gets adsorbed upon the crystal surfaces during crystallization. In the case of molecular crystals, the GU can be a monomer or a dimer of a molecule but in the present paper, we carry out calculations by assuming GUs to be monomers.

Our developed growth model is equally applicable to non-Kossel crystals, in which identical GUs occupy nonequivalent positions within the unit cell. The consequence is that different kink configurations are possible, and the energy required to

detach a GU from these different kink positions differ from one another and depends on the relative orientation of GUs in the crystal face. The crystal surface consists of flat regions called terraces and the raised partial layers called steps (see Figure 2 of the Supporting Information).³⁵ The steps themselves are also incomplete and contain several kinks. A solute molecule arriving at the surface terrace, ledge, and at the kink simply loses one, two, and three degrees of freedom, respectively. It is thus clear that the kink sites are the energetically and kinetically favored sites for the incorporation of GUs into the edge. In view of this, we have calculated the habit controlling energetics at the kink sites in order to predict growth morphology.

It is well-confirmed by detailed experiments³⁶ that spirals emanating from screw dislocations is a viable mechanism for the growth of organic crystals at low supersaturation (see Figure 3 of the Supporting Information for different growth mechanisms). Here, we assume that at a low supersaturation, growth of the *F* faces of urea and succinic acid crystals are dominated by the spiral growth mechanism, which is in accordance with experimental²² and computational results.¹⁷ Using kinetics of the molecular growth processes, we now derive an expression for the growth rate of a crystal face from solutions. In the case of solution growth, Chernov³⁷ suggested that the rate-determining step for the movement of edges is the incorporation of GUs at the kink sites. Thus, we neglect surface diffusion and only consider direct integration of GUs at the kink site. The growing and moving edges cause the spiral to rotate, facilitating continuous normal growth of the macroscopic face. In the spiral growth mechanism, the height of elementary step, $h^{(hkl)}$, of growth spiral usually corresponds to interplanar spacing, d_{hkl} , however, it depends on the symmetry elements of the underlying face. Following ref 38, we write rate of growth normal to surface $R_{\text{red}}^{(hkl)}$ as (see Figure 4 of the Supporting Information),

$$R_{\text{red}}^{(hkl)} = \mathbf{v}_{\text{step}}^{\text{kink}(hkl)} h^{(hkl)} / \lambda_0^{(hkl)} \quad (1)$$

where $\mathbf{v}_{\text{step}}^{\text{kink}(hkl)}$ and $\lambda_0^{(hkl)}$ are the lateral step velocity and step spacing, respectively. It has been shown that the structure of a step depends on supersaturation.³⁸ At finite supersaturation, step spacing for the spiral step structure is given by³⁹

$$\lambda_0^{(hkl)} \cong 19 \frac{\phi_{\text{step}}^{(hkl)} V_m}{kT \ln(1 + \sigma)} \quad (2)$$

where $\phi_{\text{step}}^{(hkl)}$ is the interfacial step energy of (hkl) face, V_m is the volume of the solute molecule, k is the Boltzmann constant, T is the temperature, and σ is the supersaturation.

We now turn to determine step velocity. It is usually assumed that the lateral step velocity is determined by the net flux of molecules entering ($N_{\text{step}}^{(hkl)}$) and leaving ($N_{\text{step}}^{\text{eq}(hkl)}$) the kink site in the step.³⁹ It depends on the way molecules are delivered at the steps.³⁷ At equilibrium, the flux of impinging molecules is equal to the flux of molecules leaving the surface. For this purpose, in accordance with ref 39, we employ the following expression for the step velocity,

$$\mathbf{v}_{\text{step}}^{\text{kink}(hkl)} = (N_{\text{step}}^{(hkl)} - N_{\text{step}}^{\text{eq}(hkl)}) a \Gamma_k \quad (3)$$

where a and Γ_k are the lattice constant and kink density, respectively. The incorporation of solute molecules are hindered by the occurrence of an ordered solvent layer near the surface known as the interfacial layer. It acts as a barrier through which solute molecules have to penetrate before they

can be incorporated into the surface.⁴⁰ Attachment of the solute would require removal of the bound solvent, which would be an additional energy barrier. $N_{\text{step}}^{(hkl)}$ is the effective flux of solute molecules seen by surface at the kink sites after penetrating the interfacial layer. It is directly proportional to the molar solute concentration,^{17,41} and thus, it is given by,

$$N_{\text{step}}^{(hkl)} \propto c \quad (4)$$

where c is the mole fraction of the solute concentration. Due to the occurrence of ordered liquid layer near the surface, not all flux of solute molecules are seen by the surface but rather a fraction of them. The growth hindrance denoted by Z depends on many factors, like equilibrium and supersaturated concentration of solute and solvent molecules,¹⁷ diffusion boundary layer thickness, and bonding energies of solute and solvent molecules to different surfaces at the kink sites. Combining the above argument with eq 4, we take the growth hindrance factor by modifying eq 4 as

$$N_{\text{step}}^{(hkl)} \propto \frac{c}{Z} \quad (5)$$

where the growth hindrance parameter, Z , can be further written as

$$Z = Z_0 + Z_{\text{interfacial-layer}} \quad (6)$$

with Z_0 and $Z_{\text{interfacial-layer}}$ are the growth hindrances provided by the surface and the interfacial layer, respectively. If there is no interfacial layer (i.e., either energy needed to remove the adsorbed solvent (fluid) molecules at the kink site on the surface ($E_{s-f}^{(hkl)}$) is tending to zero or the mole fraction of solvent (1/c) is negligible (i.e. at very high supersaturation), then the interfacial-layer hindrance vanishes ($Z_{\text{interfacial-layer}} \rightarrow 0$) and the surface-limited (Wilson–Frenkel) growth is obtained (i.e., $Z = Z_0 = c_{\text{eq}}$). Note that under this condition flux of solute and step velocity increase linearly with the supersaturation making rate of growth nonlinear with the supersaturation.⁴¹ However, it should be noted that for very high values of supersaturation, the spiral growth mechanism fails to explain the observed growth mechanism; rather the growth process adopts a 3D nucleation mechanism so that the growth rate depends linearly on supersaturation.

On the other hand, when either $E_{s-f}^{(hkl)}$ or concentration of the solvent molecules are large enough, then the hindrance experience by solute molecules from the interfacial layer dominate and, as a result, the flux of the solute molecules tends to zero.⁴² The average flux of energy delivered by the solvent molecules to the interfacial layer for its growth is given by (so that the interfacial layer can be intact) $(E_{s-f}^{(hkl)})/c$. Similarly, the average flux of energy delivered by solute molecules to the interfacial layer, in order to break it so that solute molecule can reach at the surface for growth, is given by $cE_{s-s}^{(hkl)}$, where $E_{s-s}^{(hkl)}$ is the adsorption energy of the rate-limiting solute molecules to the surface. Thus, from the above reasoning, growth inhibition experienced by the flux of solute molecules from the interfacial layer is given by

$$Z_{\text{interfacial-layer}} = \left(\frac{(1/c)E_{s-f}^{(hkl)}}{cE_{s-s}^{(hkl)}} \right) \quad (7)$$

Combining (6) and (7), we get an expression for the flux of solute seen by the crystal surface

$$N_{\text{step}}^{(hkl)} \propto \frac{c}{c_{\text{eq}} + \left(\frac{(1/c)E_{s-f}^{(hkl)}}{cE_{s-s}^{(hkl)}} \right)} \quad (8)$$

where c_{eq} is the mole fraction of solute concentration in saturated solution. Now, we turn to the determination of the step energy. The step energy is the energy required to create a one-dimensional step of height similar to that of the size of one molecule and it can be related to the local dissolution enthalpy, ΔH_{diss} , at the surface. Following the work of Liu et al.¹⁷ and Fowler et al.,⁴³ we employ the approximate expression for the average step energy given by

$$\phi_{\text{step}}^{(hkl)} n_{hkl} \approx \frac{E_{\text{slice}}^{(hkl)}}{E_{\text{latt}}} \Delta H_{hkl}^{\text{diss}} \quad (9)$$

In the above equation, E_{latt} and $E_{\text{slice}}^{(hkl)}$, denote the lattice energy per molecule of 3D and 2D crystals, respectively, and n_{hkl} is the number of neighbors of a solute molecule within the 2D slice. Note that the ordering of solvent molecules at the interface and relaxation near the surface, $\Delta H_{hkl}^{\text{diss}}$, is normally different from the bulk dissolution enthalpy. To formulate the crystal growth process at the molecular scale and considering the effect of molecular orientation of the solute molecules and surface relaxation on the adsorption energy of solute molecules, the product of slice energy and local dissolution enthalpy can be approximated as^{32a,44}

$$E_{\text{slice}}^{(hkl)} \Delta H_{hkl}^{\text{diss}} = (E_{\text{latt}} - 2E_{s-s}^{(hkl)}) \Delta H_{hkl}^{\text{diss}} \quad (10)$$

where the factor 2 is placed in eq 10 to account for the two surfaces of a slice.¹⁰ Finally, for the kink density (Γ_k), we use the expression given by⁴¹

$$\Gamma_k = \frac{2}{2 + \exp\left(\frac{\phi_{\text{step}}^{(hkl)}}{RT}\right) \left(\frac{\cosh\left(\frac{\phi_{\text{step}}^{(hkl)}}{RT} - 0.5 \ln(1+\sigma)\right)}{\cosh\left(\frac{\phi_{\text{step}}^{(hkl)}}{RT} + 0.5 \ln(1+\sigma)\right)} \right)^{1/2}} \quad (11)$$

where R is the gas constant and supersaturation (σ) is given by,⁴⁵

$$\sigma = \frac{c - c_{\text{eq}}}{c_{\text{eq}}} \quad (12)$$

Combining eqs 1–3 and 8–12, the expression for the growth rate is obtained as

$$R_{\text{red}}^{(hkl)} \propto \frac{2T d_{hkl} \ln(1+\sigma)}{\left[\left(1 - \frac{2E_{s-s}^{(hkl)}}{E_{\text{latt}}} \right) \frac{\Delta H_{\text{diss}}}{n_{hkl}} \right]} \cdot \frac{\left[\frac{c_{\text{eq}}^3 (1+\sigma)^3 E_{s-s}^{(hkl)}}{c_{\text{eq}}^3 (1+\sigma)^2 E_{s-s}^{(hkl)} + E_{s-f}^{(hkl)}} - \frac{c_{\text{eq}}^3 E_{s-s}^{(hkl)}}{c_{\text{eq}}^3 E_{s-s}^{(hkl)} + E_{s-f}^{(hkl)}} \right]}{\left(2 + \exp\left(\frac{\phi_{\text{step}}^{(hkl)}}{RT}\right) \left(\frac{\cosh\left(\frac{\phi_{\text{step}}^{(hkl)}}{RT} - 0.5 \ln(1+\sigma)\right)}{\cosh\left(\frac{\phi_{\text{step}}^{(hkl)}}{RT} + 0.5 \ln(1+\sigma)\right)} \right)^{1/2} \right)} \quad (13)$$

where c_{eq} is determined from the solubility data at the given temperature. In obtaining this expression, it is assumed that the solute concentration is uniform throughout the solution, which can be realized under intense forced convection. The detail

derivation of the above growth rate expression is given in the Supporting Information. We have employed the above expression to calculate the rate of growth of different faces of urea and succinic acid crystals as functions of supersaturation and temperature to predict growth morphologies from different media like vapor, aqueous, and methanol solutions. In the case of vapor growth (i.e., $E_{s-f}^{(hkl)} = 0$), the above expression reduces to a growth rate equation similar to that reported in ref 46. Working on the similar line of argument and keeping in mind that the crystal dissolution process is not exactly reserved to the growth process, we can develop a rate of dissolution of crystal face as function of undersaturation, temperature, solubility, and the nature of the solvent. The detailed derivation will be presented elsewhere.⁴⁷

3. COMPUTATIONAL DETAILS

We now briefly describe the computational details which we employ in this paper to calculate various energetics like $E_{s-s}^{(hkl)}$, $E_{s-f}^{(hkl)}$, and E_{latt} , in order to calculate growth rates given by eq 13 of different faces of urea and β -succinic acid crystals. For this purpose, CRYSTAL09⁴⁸ has been used. It is well-established that dispersion forces play a crucial role in determining structure and binding energies of molecular crystals. In view of this, density functional theory (DFT)-based calculations augmented with empirical dispersion terms as proposed Grimme⁴⁹ have been employed. Civalleri et al.⁵⁰ and Singh et al.⁵¹ showed that the structure and lattice energies of molecular crystals obtained using dispersion-corrected density functional theory with a B3LYP exchange-correlation functional (DFT-B3LYP-D), using a 6-31(d,p)⁵² all-electron basis set [hereafter DFT-B3LYP-D/6-31(d,p)] is in good agreement with the experimental results. In view of this, we employ the DFT-B3LYP-D/6-31(d,p) method to obtain interfacial structure and various energetics, characterizing growth of different faces of urea and succinic acid crystals. The shrinking factor of the reciprocal space net for each molecular crystal was used to define a mesh of points in the irreducible Brillouin zone, in order to meet the convergence criteria.⁵³ The level of accuracy in evaluating the Coulomb and exchange series is controlled by five thresholds,⁴⁸ and in the present calculations, the values of these are chosen to be 10^{-10} , 10^{-10} , 10^{-10} , 10^{-10} , and 10^{-20} . DFT exchange-correlation contribution is evaluated by numerical integration over the cell volume. The SCF converges when the root-mean-square (RMS) of the change in eigenvalues from two subsequent cycles is less than 10^{-10} hartree or the change in the absolute value of the total energy is less than 10^{-9} hartree.

To obtain the relaxed structure of crystals and the slices of different orientations, we choose an experimental crystal structure as the starting geometry. Using this, a full relaxation of both lattice parameters and atomic coordinates by means of analytical energy gradients⁵⁴ has been carried out. The geometry optimization of crystal structure and slices of different orientations are performed by means of a quasi-Newton optimization algorithm. Gradients are evaluated each time the energy is computed, and the second derivative matrix is updated by means of the Broyden–Fletcher–Goldfarb–Shanno algorithm. At each step, a one-dimensional minimization using a quadratic polynomial is carried out, followed by an n -dimensional search using the Hessian matrix. Geometry convergence is tested on the RMS and the absolute value of the largest component of the gradients and estimated displacements. The threshold for the maximum force, the RMS force, the maximum atomic displacement, and the RMS atomic displacement on all atoms have been set to 0.00045, 0.00030, 0.00180, and 0.00120 au, respectively. The symmetry of the slices is maintained for all the surface relaxation calculations. In order to check whether the optimized structure has reached equilibrium geometry or not, a stationary point on the potential energy surface is found, where the total force acting on atoms is numerically equal to zero. Geometry optimization is usually completed when the gradients reach the value below a given threshold. In CRYSTAL09 code, the optimization convergence is checked on the RMS and the absolute value of the largest component of both the

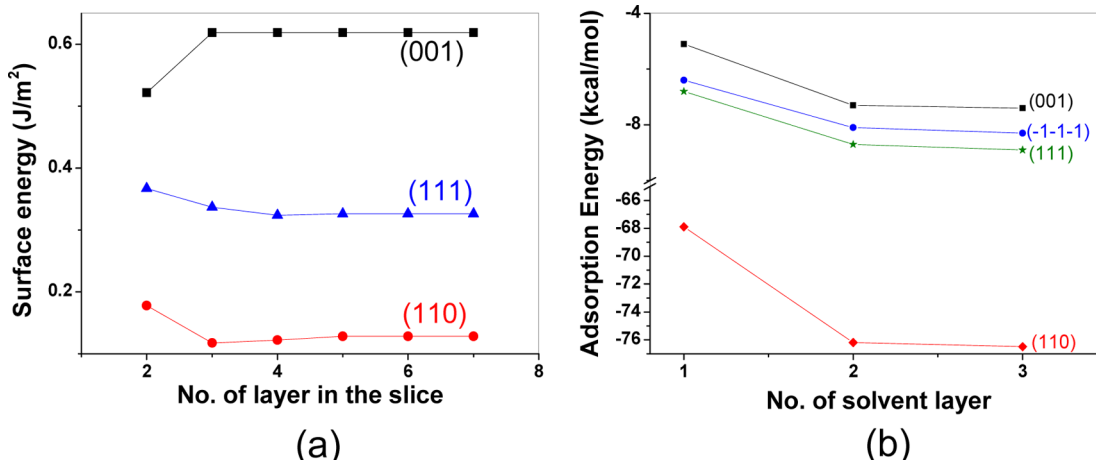


Figure 1. Convergence of (a) surface energies of (001), (110), and (111) faces of the urea crystal as function of the number of layers in different slices of orientation and (b) adsorption energy of strongly bound water molecules to (001), (110), (111), and ($\overline{1}\overline{1}\overline{1}$) surfaces of urea crystal obtained using DFT-B3LYP-D/6-31G(d,p).

gradients and the estimated displacements. The structural optimization is successfully completed when all four conditions set by the above thresholds are simultaneously satisfied. The symmetry of the crystals and slices were maintained during the optimization process.

An empirical correction term to include long-range dispersion interactions in DFT methods as proposed by Grimme⁴⁹ has been implemented in the CRYSTAL09 code. It is a damped pairwise London-type term given by,

$$E_{\text{disp}} = -s_6 \sum_{i=1}^{N_{\text{at}}-1} \sum_{j=i+1}^{N_{\text{at}}} \sum_g \frac{C_6^{ij}}{R_{ij,g}^6} \left(\frac{1}{1 + e^{-d(R_{ij,g}/R_{\text{vdw}} - 1)}} \right) \quad (14)$$

where the summation is over all pairs of atom and g lattice vectors with the exclusion of self-interaction ($i = j$) for $g = 0$. C_6^{ij} is the dispersion coefficient, and R_{ij} is the interatomic distances between atom i^{th} in the reference cell and j^{th} in the neighboring cell. R_{vdw} is the sum of the van der Waals radii, and d is the steepness of the damping function. The values of C_6 , R_{vdw} , and d were taken from ref 49. The scaling factor, s_6 , depends on the adopted exchange-correlation functional ($s_6 = 1.05$ for B3LYP method⁴⁹). A cutoff distance of 25.0 Å was used to truncate the summation over lattice vectors to obtain precision on the order of 0.02 kJ mol⁻¹ in the calculation of dispersion energy. The dispersion correction is applied to the computed ab initio total energy and their gradients at all levels of the theory. We have carried out total energy calculations and geometry optimization with and without including the empirical dispersion correction, in order to ascertain the effect of dispersion forces on the structure and lattice energy. It has been shown that the inclusion of dispersion forces is crucial to properly model the weak intermolecular interactions that play an important role in determining the molecular structure of crystalline urea.^{50–55} Since in the present calculations we have used a Gaussian-type of finite basis sets, particular attention has been paid to the basis set dependence and the effect of basis set superposition error (BSSE) on the structure and the lattice energy of hydrogen-bonded molecular crystals.

Having discussed the computational details, we now describe the procedure to construct slices of different orientations and interfacial structures required to obtain various interfacial energetics in order to calculate growth rate. The following methodology has been adopted to construct the slices of different crystallographic orientations from the projection of bulk structures of urea and succinic acid crystals. The charge neutrality of the slice was maintained during the process of slice generation. The structure of slice with minimum energy configuration is obtained very carefully. If the molecule has a dipole moment, attention must be paid to the surface termination because a slice can possess a net dipole perpendicular to the surface. The stability of a slice depends on its orientation (hkl), number of atomic layers, correct surface termination, and surface relaxation/reconstruction. The

number of atomic layers in a slice is determined by the convergence of the surface energy and in order to maintain the stoichiometry, we have taken all atomic layers contained in the slice of thickness nd_{hkl} where n represents the number of layers in the slice. Figure 1a shows the convergence of surface energy of different faces of the urea crystal as a function of the number of layers. It clearly shows that at least three layers are needed to obtain a converged value of the surface energy of the different faces of the urea crystal. While creating a slice, often more than one surface termination is possible. To identify the correct surface termination of the slice, the above-discussed criteria is used. In most cases, these conditions are satisfied at the same configuration. Details of the construction of different slices from the projection of crystallographic structure of urea crystal are reported in ref 32.

To model the different crystal–solution interfaces of urea crystal, the following set of calculations were carried out. First, the structure of urea–water molecules in various configurations were obtained with the help of Molden Graphical package,⁵⁶ and structural optimizations were carried out using CRYSTAL09 code.⁴⁸ With the positional disorder characteristic of the solvent molecules adsorbed on the crystal surface kept in mind, several positions and orientations of the solvent molecules have been tried before obtaining stable configurations. Figures 2 (panel a–d) and 3 (a–d) show the optimized structures of

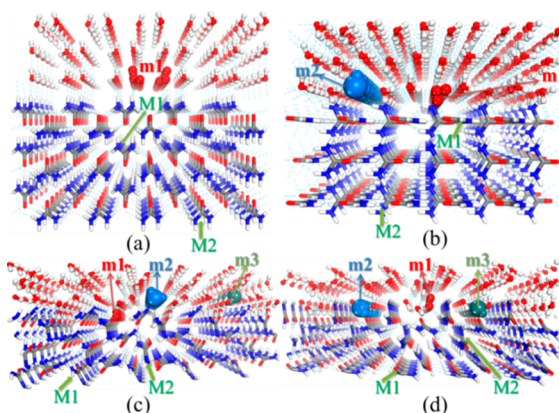


Figure 2. The structurally optimized crystalline urea–water interfaces of (a) (001), (b) (110), (c) (111), and (d) ($\overline{1}\overline{1}\overline{1}$) surfaces. The water molecules are adsorbed at the surfaces and specifically, the strongest adsorbed water molecules are shown by a red ball and stick and “m1” labels. Other water molecules of m2 and m3 orientations are shown by blue and green color, respectively. Urea molecules of different orientations at the crystal faces are labeled by M1 and M2.

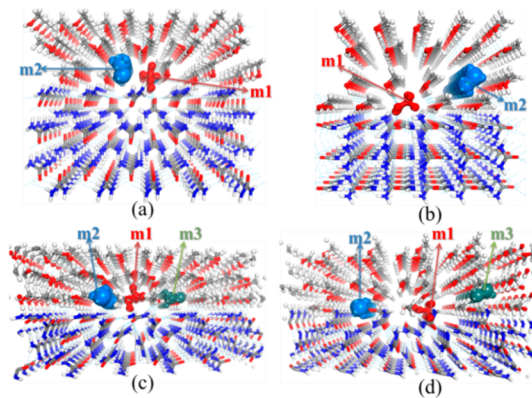


Figure 3. The optimized interfacial structure of the urea–methanol interfaces of (a) (001), (b) (110), (c) (111), and (d) (111) surfaces. The specifically strongest adsorbed water molecules are shown by a red ball and stick and m1 labels. Other water molecules of m2 and m3 orientations are shown by blue and green, respectively. The adsorption energy of the m2 molecule is higher than that of m3.

urea–water and urea–methanol for (a) (001), (b) (110), (c) (111), and (d) (111) interfaces, respectively. We have considered the polarity of the various faces of the urea crystal in order to study the interactions of solvent molecules to these faces. The polarity of a face is determined by its atomic structure, in particular, by the atoms which are exposed at the interface and are easily accessed by the solvent molecules. Hydrated models of urea–water interfaces have been examined by positioning three layers of water molecules above the surface and then allowing the surface and solvent molecules to relax to their minimum energy configuration.

A similar study for methanol layers over the urea surface has also been carried out. Since ordering of the solvent is strongest near the surface and vanishes toward the bulk liquid, we assume that the liquidlike behavior of loosely bonded solvent molecules to the crystal surfaces do not govern the growth rate, and hence, we do not include them in growth rate calculations. Thus, it is expected that strongly bonded solvent molecules should be closest to the surfaces. To calculate adsorption energy of the strongly adsorbed solvent molecule at different faces of urea crystal, three layers of solvent molecules are placed over the surfaces of (001), (110), (111), and (111) faces, and these structures are then optimized. The convergence of the adsorption energies of strongly adsorbed solvent molecule on the different surfaces is shown in Figure 1b, which clearly reveals that at least three layers of solvent are required to obtain the convergence in the value of $E_{s-f}^{(hkl)}$. We note here that the optimized interfacial structures of urea and water are in agreement with the results obtained from molecular dynamic simulations by Boek et al.⁵⁷

4. RESULTS AND DISCUSSION

We begin with the discussion of the results of the crystal structure and lattice energy of urea and succinic acid crystals. In this respect, we have carried out periodic ab initio density functional calculations to study the role of dispersion interactions and analyzed the relevance of BSSE in the prediction of structure and lattice energy. The lattice energy per molecule, E_{latt} , is given by

$$E_{\text{latt}} = \frac{E_{\text{crystal}}}{N} - E_{\text{molecule}} + E_{\text{BSSE}} \quad (15)$$

where E_{crystal} is the total energy per unit cell and N is the number of molecules in a unit cell, E_{molecule} is the energy of molecule and E_{BSSE} is the term which takes into account the energy correction arising due to the BSSE. The energy of molecule with BSSE correction has been calculated by placing 90 ghost atoms in a cluster surrounding the molecule at the atomic positions obtained from the optimized crystal structure at the same computational level. This is how we eventually calculate the lattice and adsorption energies of solute and solvent molecules attached to different surfaces. The calculated lattice energy is compared with the corresponding experimental data, which are related to the enthalpy of sublimation, ΔH_{sub} . The lattice energy and sublimation enthalpy are related to each other by the following expression,⁵⁸

$$E_{\text{latt}} = -\Delta H_{\text{sub}} - 2RT \quad (16)$$

where R and T are the gas constant and temperature, respectively, and the $2RT$ factor is the commonly accepted correction⁵⁹ to account for the zero-point energy and thermal corrections at 298 K. The experimental value of lattice energy of urea and succinic acid crystals has been estimated by the above equation from the data on sublimation enthalpy available in the literature.

In Table 1, we compile the optimized lattice parameters and lattice energy of urea and β -succinic acid crystals obtained using DFT-B3LYP-D/6-31G(d,p) level of theory. The results for % deviation in lattice parameters and lattice energy from the corresponding experimental data (shown in parentheses) of different crystals clearly show that the results are in close agreement with the corresponding experimental data.^{60–63} It is evident from Table 1, that the error in lattice energies and lattice parameters are below 1% and 6.2%, respectively, with respect to the experimental values. It has been shown that the DFT-B3LYP method, without taking into account the dispersion interaction, gives results which are rather poor in

Table 1. Experimental and Calculated Lattice Cell Parameters and Lattice Energy with Their % Deviations from the Corresponding Experimental Data (In Parentheses) of Urea and Succinic Acid Crystals at the DFT-B3LYP-D/6-31G(d,p) Level of Theory

crystal	experimental values of		calculated values of				
	lattice energy ^{62,63} corrected at 0 K using eq 16 (kJ mol ⁻¹)	lattice cell parameters ^{60,61}	lattice energy (kJ mol ⁻¹)	lattice cell parameters			
				a (Å)	b (Å)	c (Å)	β (°)
urea	-103.6	$a = 5.661 \text{ \AA}$ $c = 4.712 \text{ \AA}$ $a = 5.519 \text{ \AA}$	-104.3 (-0.7%)	5.677 (0.3%)	5.677 (0.3%)	4.674 (-0.8%)	
β -succinic acid	-137.4	$b = 8.862 \text{ \AA}$ $c = 5.101 \text{ \AA}$ $\beta = 91.590^\circ$	-136.5 (1.0%)	5.385 (2.4)	8.394 (5.3)	4.784 (6.2)	95.997 (-4.8)

quality with respect to the experimental data.⁵⁰ The contribution of dispersion energy to the total lattice energy of urea and succinic crystals are 42% and 54%, respectively. Thus, inclusion of dispersion interactions significantly improves the calculations of lattice energy and lattice parameters of the molecular crystals. In view of this, the structures of different interfacial layers and the bonding energies of solute and solvent molecules to the various surfaces have been calculated using the DFT-B3LYP-D/6-31G(d,p) level of theory. Here, we note that the periodic local-MP2 (LMP2) method is capable of producing more accurate results⁶⁴ for the dispersion energy compared to the DFT-based method augmented with an empirical dispersion term as implemented in CRYSTAL09 code. However, the calculations of adsorption energies of solute–surface and solvent–surface involving more than 400 atoms are computationally expensive at the LMP2 level of theory.

4.1. Solvent-Induced Habit Modification of Molecular Crystals: Role of the Crystal–Solution Interface. As we have discussed earlier, the solvent and external growth parameters greatly affect the growth rate of the crystal faces and hence the crystal morphology. In this context, we have chosen two molecular crystals, namely, urea and β -succinic acid, to study the role of solvents and external growth factors like solubility, temperature, and supersaturation on the morphology of these crystals.

4.1.1. Crystal Growth Morphology of Urea Crystal from Aqueous and Methanol Solutions. Having discussed the results for lattice parameters and lattice energy, we now turn to calculate the growth rate of different faces of urea crystal from aqueous and methanol solutions to simulate the growth morphology of a urea crystal as a function of supersaturation, temperature, and different solvents. Urea [$\text{O}=\text{C}(\text{NH}_2)_2$] belongs to the tetragonal, noncentrosymmetric $P\bar{4}2_1m$ space group, with two molecules in the unit cell.⁶⁰ When grown from aqueous solution, urea crystallizes as a long thin prism with a large aspect ratio (~ 50). The aspect ratio decreases when methanol is used as a solvent to grow urea crystal. The prediction of growth shape of the urea crystal from aqueous and methanol solutions have attracted considerable attention. In this direction, prominent works have been done by Liu et al.,¹⁷ Doherty et al.,¹⁹ and Gale et al.,²¹ which are briefly described in Introduction.

We now focus our attention on the study of the growth rate and shape of the urea crystal from aqueous and methanol solutions. To this end, we consider (001), (110), (111), and $(\overline{1}\overline{1}\overline{1})$ faces to calculate $E_{s-f}^{(hkl)}$ and $E_{s-s}^{(hkl)}$. It is well-known that the growth rate of a high index face is higher than that of a low index face and generally not expected to appear in growth morphology. Consequently, we have not considered high index faces, other than the above-mentioned faces for calculating growth morphology of the urea crystal. It is evident from Figure 1 that the surface and adsorption energies of solvent molecules at the above faces converge after three layers. Consequently, we have taken $3d_{hkl}$ thick slabs and 3 solvent layers of the above-mentioned faces, in order to obtain interfacial structures and solute–surface and solvent–surface energetics. The optimized interfacial structures of the different faces of the urea crystal from aqueous and methanol solutions have been employed for the calculations of $E_{s-s}^{(hkl)}$ and $E_{s-f}^{(hkl)}$, which are displayed in Figures 2 and 3, respectively. The calculated values of $E_{s-s}^{(hkl)}$ and $E_{s-f}^{(hkl)}$ and the corrected values of $E_{s-f}^{(hkl)}$ are tabulated in Table 2. The energy correction in $E_{s-f}^{(hkl)}$ is made for a single H-bond

Table 2. The Bonding Energies of Solute–Surface and Solvent–Surface of Strongly Adsorbed Water and Methanol Molecule at Different Faces of Urea Crystal by DFT-B3LYP-D/6-31G(d,p)^a

crystal faces (<i>hkl</i>)	$E_{s-f}^{(hkl)}$ (kJ mol ⁻¹) of solute molecule in orientation			
	water molecule in orientation		methanol molecule in orientation	
	M1	M2	m	m
(001)	-18.8	-33.4	-7.4 (-1.7)	-21.3 (-10.5)
(110)	-12.1	-19.9	-76.5 (-70.8)	-126.5 (-115.6)
(111)	-30.3	-19.0	-8.9 (-3.2)	-42.2 (-31.3)
$(\overline{1}\overline{1}\overline{1})$	-34.3	-23.4	-8.3 (-2.5)	-37.6 (-26.8)

^aThe periodic supercell model has been utilized to compute various interactions and corrected values⁶⁵ of $E_{s-f}^{(hkl)}$ and are reported in parentheses. Convergence of $E_{s-f}^{(hkl)}$ was achieved by increasing the supercell size, as shown in Figure 4.

energy of -5.8 kJ mol⁻¹ for icelike water molecules and of -10.9 kJ mol⁻¹ for a methanol molecule.⁶⁵ The corrected bonding energies of solvent molecules are shown in parentheses in Table 2. It is clear from Table 2 that the adsorption energy of the rate-limiting molecule on the $(\overline{1}\overline{1}\overline{1})$ face is higher than that of the (111) face of the urea crystal. Consequently, the growth rate of the $(\overline{1}\overline{1}\overline{1})$ face is higher than that of the (111) face. We note here that detailed study of the asymmetrical growth and dissolution at the opposite and hemihedral faces like the (111) and $(\overline{1}\overline{1}\overline{1})$ faces of the urea crystal from the vapor phase is presented elsewhere.⁵¹ It is also evident from Table 2 that the vapor growth rate of (111) and $(\overline{1}\overline{1}\overline{1})$ faces are rate-determined by the adsorption of M2-oriented GU. On the other hand, adsorption of M1-oriented GU rate limit the growth of (001) and (110) faces. It is evident from Table 2 that the adsorption energy of M1-oriented GU is approximately two times lower than the adsorption energy of M2-oriented GU to the (001) face. Thus, the growth rate of M1-oriented GU to the (001) face provides a rate-determining step. The schematic illustration of the adsorption of M1- and M2-oriented GUs on the (001) face of the urea crystal is shown in Figure 5 of the Supporting Information. Table 3 lists the bonding energies of other weakly bound solvent molecules to (111) and $(\overline{1}\overline{1}\overline{1})$ surfaces of the urea crystal. The bonding energies of the solvent molecule to the different faces were calculated by constructing supercells of various sizes. Convergence of bonding energies of water molecules to the different crystal surfaces as a function of size of the supercell is shown in Figure 4. Figures 5 and 6 show the growth rate of different faces of urea crystal from aqueous and methanol solutions by the adsorption of the rate-limited solute molecule, respectively, versus supersaturation (σ) at different saturation temperatures.

It is evident from Figures 5 and 6 that the growth rate is nonlinear in the low σ regime, while it is linear for large values of σ . The results are consistent with the growth rate measurement of Davey et al.²² It is also clear from these figures that the growth rate ($R_{\text{red}}^{(110)}$) of the (110) face is one order smaller than the growth rates of the (001) and (111) faces in the low σ regime, which is in agreement with the experimental result.²² It is evident from Table 2 that the

Table 3. Bonding Energies (in kJ mol^{-1}) of Other Weakly Bonded Water and Methanol Molecules with (111) and ($\bar{1}\bar{1}\bar{1}$) Faces of Urea Crystal by DFT-B3LYP-D/6-31G(d,p)^a

crystal face (hkl)	$E_{s-f}^{(hkl)}$ (kJ mol $^{-1}$)				
	water molecule in orientation		methanol molecule in orientation		
	m2	m3			
(111)	-7.5 (-1.73)	-6.4 (-0.63)	-25.1 (-14.2)	-22.3 (-11.4)	
($\bar{1}\bar{1}\bar{1}$)	-6.8 (-1.0)	-6.3 (-0.5)	-24.5 (-13.6)	-20.8 (-9.9)	

^aThe corrected values of $E_{s-f}^{(hkl)}$ are reported in parentheses.

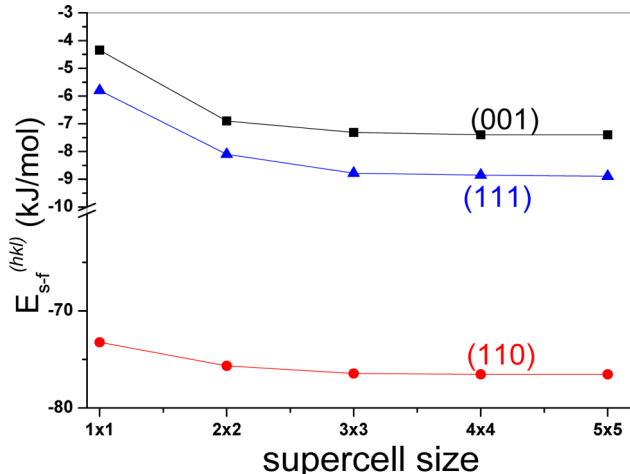


Figure 4. Convergence of adsorption energies of water molecules on different crystal surfaces of the urea crystal, as function of the size of the supercell.

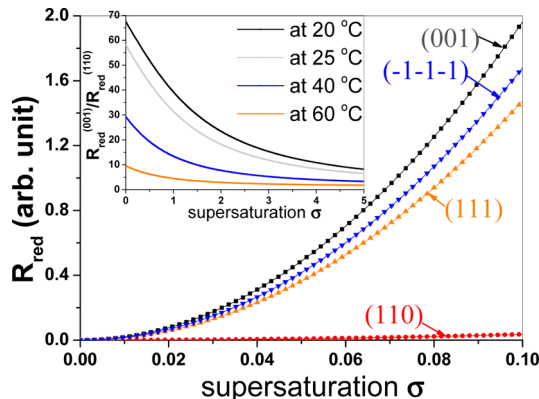


Figure 5. Calculated growth rates of (001), (110), (111), and ($\bar{1}\bar{1}\bar{1}$) faces of the urea crystal vs σ at 25 °C from the aqueous solution. The aspect ratios ($R_{\text{red}}^{(001)}/R_{\text{red}}^{(110)}$) vs σ at different saturation temperatures are shown in the inset. The habit of the urea crystal becomes needlelike for low values of σ .

adsorption energy of water/methanol molecules to the (110) face is one order stronger than (001) and (111) faces, in agreement with the others computational results.²¹ Figure 7 shows the relative increase in growth rates of (a) (001) and (b) (110) faces compared to the growth rate at 20 °C of the urea crystal from aqueous solution vs σ , at different temperatures. It is clear from Figure 7 that the % of increase in the rate of growth of the (110) face is approximately two orders higher than that of the (001) face. The huge increase in growth rate of the (110) face with temperature may be ascribed to the roughening of the interface. The solvent–surface interaction of the (110) surface is one order higher than the (001), (111), or

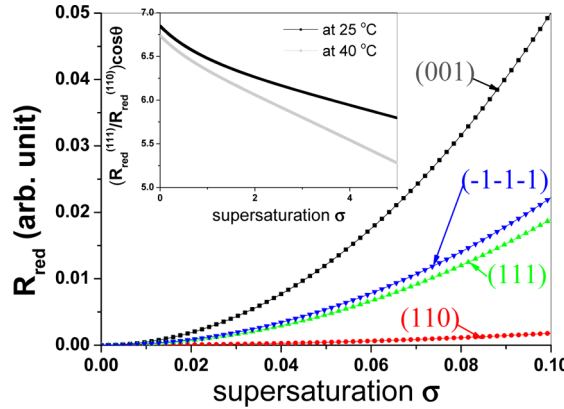


Figure 6. Calculated growth rates of (001), (110), (111), and ($\bar{1}\bar{1}\bar{1}$) faces of the urea crystal vs σ at 25 °C from the methanol solution. The aspect ratios (length to breadth) vs σ at different saturation temperatures are shown in the inset. Growth rate in the [001] direction is given by $R_{\text{red}}^{(001)}\cos\theta$, where θ denotes the interfacial angle between the (001) and the (111) faces.

(111) faces and, hence, the (110) surface is rougher than other faces. Consequently, growth of the (110) face is two orders slower than the (001), (111), and ($\bar{1}\bar{1}\bar{1}$) faces. The stronger interaction of water and methanol molecules to the (110) surface is also responsible for the solvent trapping to this face, which is experimentally observed during the growth commonly known as solvent trapping to the face. It is interesting to observe that at a relatively higher temperature and supersaturation, $R_{\text{red}}^{(110)}$ increases rapidly, which is in agreement with the growth rate calculations by Piana et al.²¹ The aspect ratio ($AS = R_{\text{red}}^{(001)}/R_{\text{red}}^{(110)}$) as a function of σ at different saturation temperatures from aqueous and methanol solutions are shown in the insets of Figures 5 and 6, respectively. Our results show that an increase in σ results in a decrease of the aspect ratio. This observation is analogous with the growth shape calculation of α -glycine from aqueous solution.¹⁸ Figure 8 shows the experimental growth rate,²² as fitted to the BCF model for (001) and (110) faces of urea crystal from aqueous solution at 25 °C. The experimental aspect ratio is shown in the inset of Figure 8, which clearly reveals that the elongation decreases upon increasing the supersaturation. Under low supersaturation, it has been shown that the experimental growth rate data of the (001) face is best represented by the BCF model.²² We have employed the BCF model²⁰ to fit the experimental growth rate data of the (110) face because Piana et al.²¹ showed that in the aqueous solution, growth of the (110) face is limited by nucleation. On the other hand, growth rate of the (110) face from the methanol solution can be represented by the birth-spread model. The increase in saturation temperature results in an increase in the growth rate but a decrease in the aspect ratio. This happens because the net difference between the fluxes of

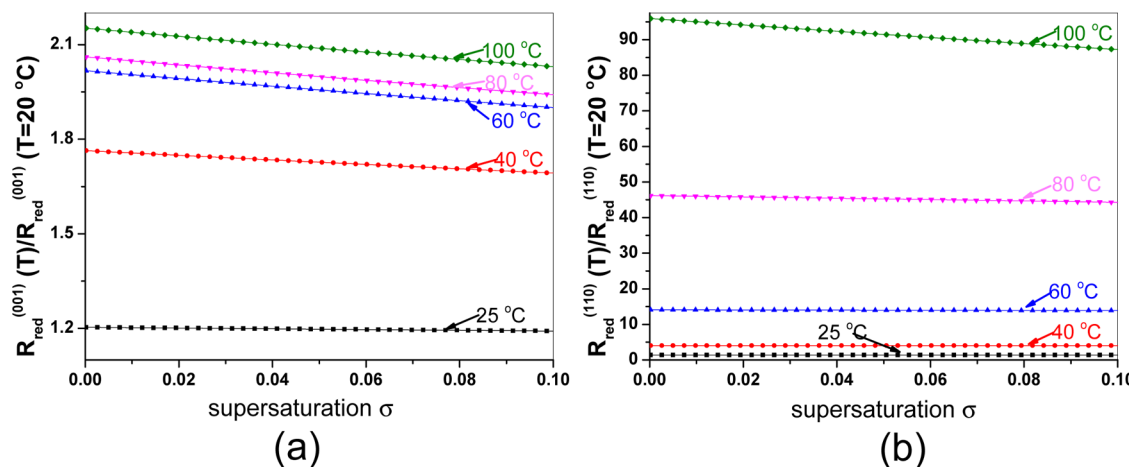


Figure 7. Calculated relative increase in the growth rate of $[R(T)/R(T = 20^\circ\text{C})]$ of the (a) (001) and (b) (110) faces of urea crystal vs σ , at different temperatures from the aqueous solution.

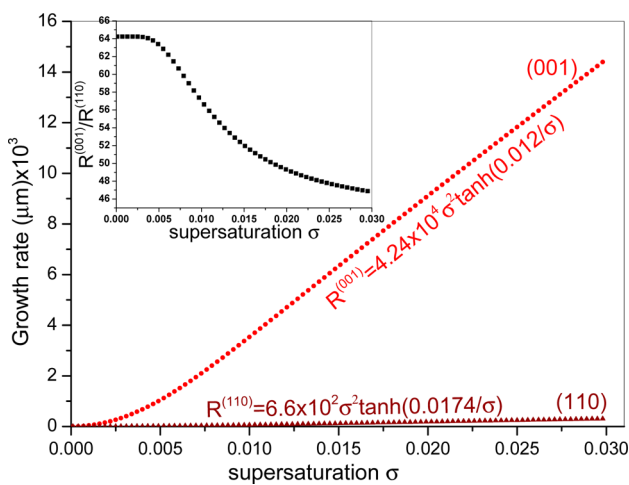


Figure 8. Experimental growth rate data of (001) and (110) faces of urea crystal from aqueous solution at 25 °C were fitted with the BCF model. The aspect ratio as a function of supersaturation of the urea crystal from the aqueous solution is shown in the inset.

solvent molecules to the (110) and (001) surfaces decreases by increasing σ . It is clear from Table 2 that the (110) face has more affinity for water and methanol than other faces. The relative methanol-surface interactions at the (110) and (001) faces is significantly lower than that of water. Also, due to decreased solubility of urea in methanol than that in water further leads to a decrease in aspect ratio. This behavior is in accordance with the experimental observations. Thus, we conclude that the growth mechanism for the (110) surface is different from those of the (001), (111), and ($\overline{1}\overline{1}\overline{1}$) faces.

To further establish the validity of our approach, we compare our simulated growth rate results with the corresponding experimental measured results. Figure 9 shows the comparison of our computed growth rate of the (001) face from the aqueous solution, as a function of supersaturation at 25 °C with the experimentally measured growth rate.²² The proportionality constant in the growth rate eq 13 for the urea crystal is evaluated by comparing the simulated growth rate with the experimentally measured growth rate for each supersaturation. The calculated value of the constant is found to be 11.67 for the (001) face. It can be observed from Figure 9 that the calculated rate of growth of the (001) face is in good agreement with the

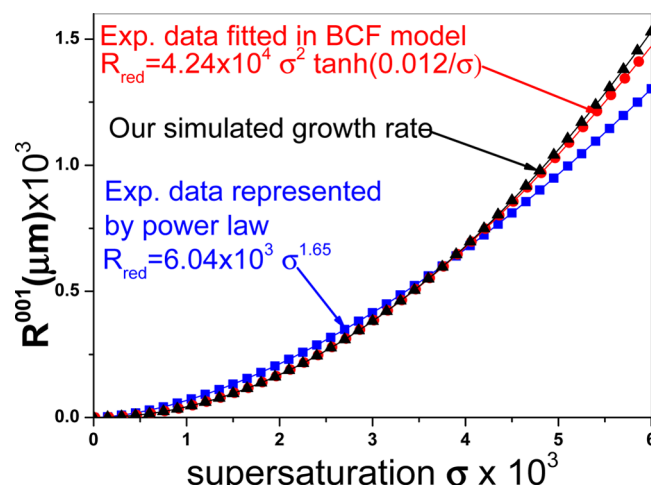


Figure 9. Experimental and calculated growth rate of the (001) face of the urea crystal obtained from aqueous solution, as a function of supersaturation at 25 °C.

experimentally measured rate of growth. The predicted growth habits of aqueous and methanol grown urea crystals are shown in Figure 10 (panels b and c), respectively, for low values of σ and at a temperature of 20 °C, which are in agreement with the experimental results.^{23,22} For completeness, we show the growth habit of the urea crystal grown from the vapor phase in Figure 10a. It is clear from Figure 10 (panels b–c) that the

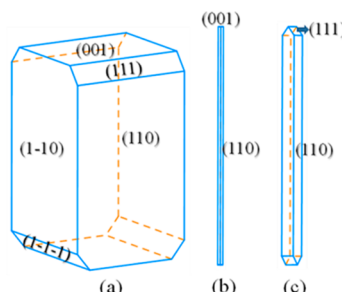


Figure 10. Predicted growth habits of the crystalline urea from the (a) vapor phase and (b) aqueous solution at low σ at 20 °C and the (c) methanol solution at low σ at 25 °C. The calculated aspect ratio from the aqueous and methanol solutions are 57 and 7, respectively.

aspect ratio decreases when water is replaced by the methanol, which is consistent with the experimental observations.

4.1.2. Prediction of Crystal Growth Morphology of β -Succinic Acid Crystal from Aqueous and Isopropanol Solutions. Having studied the growth morphology of the urea crystal from vapor, aqueous, and methanolic solutions, we now focus our attention on the study of growth morphology of β -succinic acid crystals from vapor, aqueous, and isopropyl alcohol solutions by employing eq 13 for growth rate expression. The experimental crystal morphology of β -succinic acid grown from vapor has a predominant (010) face and smaller (100), (111), (110), and (011) faces. These observations are in good agreement with the shapes predicted by the extended HP model, which takes into account the molecular orientation on growth shape.^{32a} When succinic acid crystals are grown from aqueous solution, the crystal morphology has a predominant (100) basal face bounded by the (010), (011), and (111) planes.²⁸ The needle-shape crystal morphologies have been obtained when they are grown from an isopropyl alcohol solution.²⁸

We now present the results for the growth rate and morphologies of the β -succinic acid crystal from aqueous and isopropyl alcohol solutions. For this purpose, according to the available experimental and theoretical results, we consider the (100), (111), (011), (010), and (110) faces. Figure 11 (panels

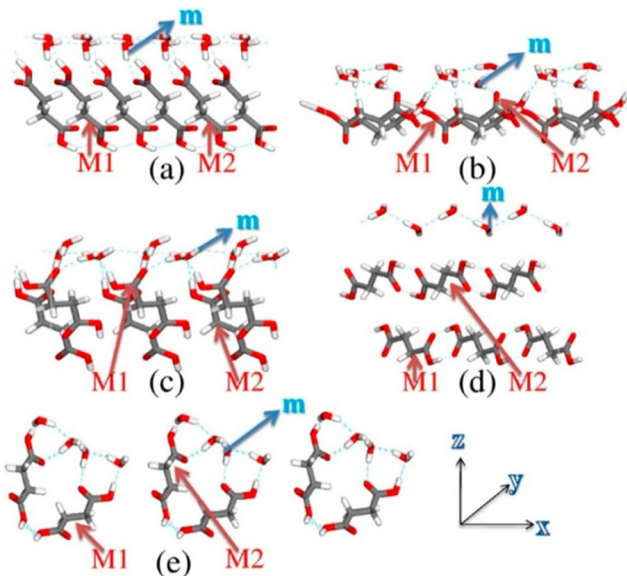


Figure 11. The optimized atomic structure of the crystal–water interfaces of the (a) (100), (b) (111), (c) (011), (d) (010), and (e) (110) surfaces of the succinic acid crystal. The water molecules adsorbed at the crystal surfaces and the strongest-bound water molecules are labeled m and shown by an arrow. Solute molecules of different orientations in the crystal faces are labeled M1 and M2.

a–e) shows the optimized atomic structures of the above-mentioned succinic acid crystal–water interfaces. The strongly adsorbed water molecules are labeled m in Figure 11. We have calculated the total energy (E_1) of a 5×5 supercell constructed from the optimized interfacial structures, as shown in Figure 11. The strongly adsorbed water molecule at the kink site is removed from the above constructed supercell, and the total energy of this structure (E_2) has been calculated. The intramolecular energy of a water molecule (E_3) in liquid water has also been calculated to obtain $E_{s-f}^{(hkl)}$, by using the

relation $E_{s-f}^{(hkl)} = (E_1 - E_2 - E_3)$. In Table 4, we list adsorption energies of solute–surface and solvent–surface of strongly

Table 4. Adsorption Energies of Solute–Surface and Solvent–Surface of Strongly Adsorbed Water and Iso-Propanol Molecules at Different Faces of the Succinic Acid Crystal Using the DFT-B3LYP-D/6-31(d,p) Method

crystal face (hkl)	$E_{s-s}^{(hkl)}$ (kJ/mol) of orientation		$E_{s-f}^{(hkl)}$ (kJ/mol) of		
			water–succinic acid		isopropyl alcohol–succinic acid
	M1	M2	uncorrected	corrected	corrected
(100)	-25.1	-21.3	-29.7	-23.8	-26.3
(111)	-25.9	-27.6	-20.9	-15.0	-3.3
(011)	-41.0	-41.4	-24.2	-18.8	-43.1
(010)	-31.4	-31.4	-15.9	-10.0	-158.8
(110)	-31.4	-35.1	-19.2	-13.4	-79.4

bound water and isopropyl alcohol molecules. The energy correction is made for a single hydrogen bond energy (-5.8 kJ/mol) of the water molecule in the liquid water.⁶³ Figure 12

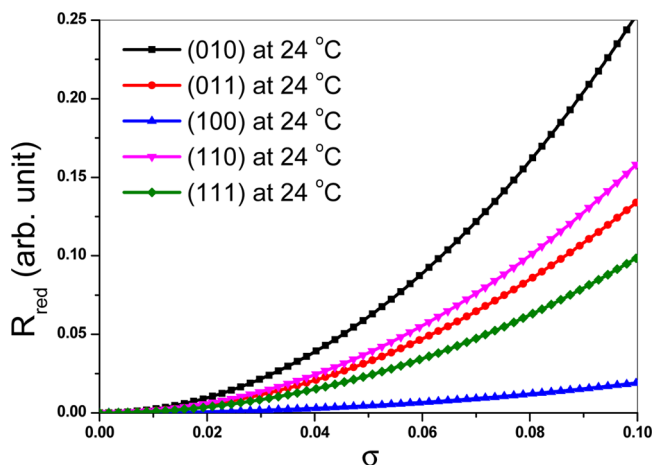


Figure 12. Reduced growth rate of (100), (111), (011), (010), and (020) faces of succinic acid crystal vs σ , at 24 °C, from the aqueous solution.

shows the aqueous growth rate as a function of σ , at 24 °C. It reveals that the rate of growth of (010) ($R_{\text{red}}^{(010)}$) is the largest, while the growth rate of (100) is the smallest, which is in agreement with the experimental observation.^{25,28} Our calculation predicts that the aqueous morphology of the succinic acid crystal is nearly independent of both the supersaturation and the saturation temperature. An increase in the saturation temperature results in an increase in the rate of growth, but the shape of the succinic acid crystal remains unchanged. The growth rates of all the above faces of succinic acid crystal increase by a factor of 8, when the saturation temperature is increased from 24 to 40 °C.

The calculated morphology of aqueous grown succinic acid crystal is shown in Figure 13b, which is in agreement with the experimental results.^{25,27} The growth rate of different faces of the succinic acid crystal from isopropyl alcohol solution as a function of σ at 24 °C is shown in Figure 14. It clearly shows that the growth rate of the (011) face is the highest and that of the (100) face is the lowest, which is in accordance with the

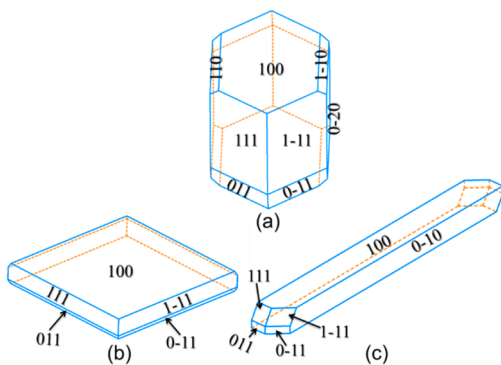


Figure 13. Predicted growth morphologies of β -succinic acid crystals of (a) vapor grown, (b) aqueous, and (c) isopropyl alcohol solutions at low values of σ .

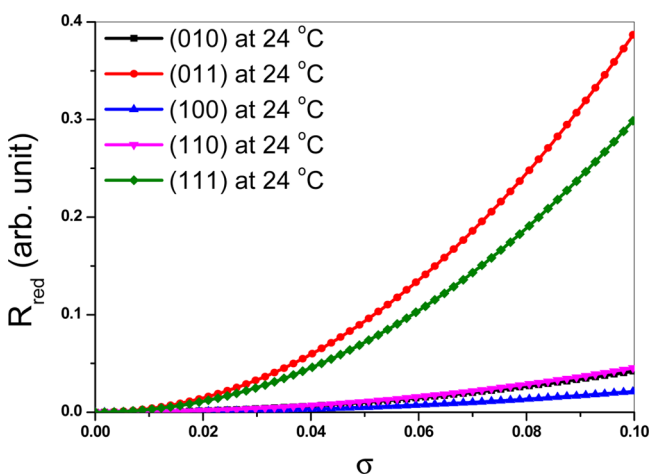


Figure 14. Reduced growth rate of the (100), (111), (011), (010), and (010) faces of succinic acid crystal vs σ , at 24 °C, grown from the isopropyl alcohol solution.

experimental observation.²⁸ The growth rates of all the faces increases with saturation temperature, but the morphology of the crystal remains unchanged. It has been found that the calculated growth rates of all the faces increase by a factor of 4 when saturation temperature increased from 24 to 40 °C. The shape of the succinic acid crystal obtained from isopropyl alcohol solution is shown in Figure 13c, which is in agreement with the experimentally observed morphology.²⁸ The growth rates of all the faces are lower in isopropyl alcohol than aqueous solutions. The growth rate of (010) and (100) are reduced by a factor of 7, when aqueous solution is replaced by isopropyl alcohol solution, which is consistent with the reported results available in the literature.²⁸ The experimental observations confirm that crystal growth takes place more slowly in isopropyl alcohol than in aqueous solution. It is attributed to the stronger adsorption of isopropyl alcohol molecules than the water molecules onto the growing surfaces. It is clear from Figures 12 and 14 that the growth rate of the (010) face is higher than the (100) face in both the solvents, agreeing with the experimental growth rate studies carried out by Davey et al.²⁸ For completeness, we also show the growth habit of the vapor-grown β -succinic acid crystal in Figure 13a. The calculated adsorption energies of water and isopropyl alcohol solvents on the growing crystal surfaces are well-supported by the experimental results,²⁸ that succinic acid does not strongly interact within the three-dimensional water structure; rather, it

prefers to form intra- and intermolecular hydrogen bonds. However, the structure of isopropyl alcohol is more open to the succinic acid molecules and interactions among them are relatively stronger. This is confirmed by the measurement of the solubility of succinic acid as a function of the dielectric constant of solutions in a series of alcohols.²⁸ In conclusion, it can be stated that succinic acid–isopropyl alcohol interactions are stronger than succinic acid–water interactions.

5. CONCLUSIONS

In summary, we have investigated the role of solvents and other external growth factors in predicting the growth morphologies of two molecular crystals, namely, urea and β -succinic acid crystals, at low supersaturation. In this respect, we have established a growth rate expression, which takes into account various energetics characterizing solute–surface and solvent–surface interfaces and external growth parameters within the framework of the spiral growth mechanism. The growth expression presented in this paper is based on the inhibition mechanism which enables us to incorporate the effect of many internal and external growth parameters, such as molecular orientation, surface relaxation, interplanar distance, coordination number, solubility, temperature, supersaturation, and the nature of solvents, on the rate of growth. The formation of an interfacial structure occurs due to the ordering of the solvent at the surface, which slows down the growth rate of the crystal face. An Ab initio periodic dispersion corrected DFT-B3LYP method has been employed to obtain interfacial structures and bonding energies of various solute–surface and solvent–surface interfaces, associated with the above-mentioned crystals. The effects of molecular orientation of GUs and surface relaxation of the habit faces have also been considered in order to identify the adsorption of rate-determining molecules. The approach is applied to predict the crystal growth shapes of the crystals from vapor and different solvents. Our results predict the block- and needlelike habits of the urea crystal, resulting from vapor and aqueous/methanol solution, respectively. The present study clearly shows that the aspect ratio of the urea crystal decreases with increasing growth temperature and supersaturation, which is consistent with the experimental observations. The aspect ratio decreases further when a less polar solvent like methanol is used as a solvent rather than water. It is due to the lesser interaction of methanol with the (110) face compared to that of water. Our results show that the (110) face has more affinity with water and methanol than other faces. The relative methanol–surface interactions at the (110) and (001) faces are significantly lower than that of water. Also, due to the reduced solubility of urea in methanol than that in water further leads to a decrease in the aspect ratio. Thus, on the basis of our results, we anticipate that the use of solvents having lower polarity than methanol will lead to blocklike crystal morphology. Further work in this direction is currently in progress.

The growth morphologies of β -succinic acid crystals from vapor, aqueous, and isopropyl alcohol solutions are in good agreement with the corresponding experimentally obtained shapes. The predicted growth morphologies of these crystals reproduce all the experimentally observed faces, which clearly demonstrate the validity of the crystal growth model presented in this paper. The remarkable agreement between the predicted growth morphologies and the corresponding experimental results allows us to understand the role played by solvents and other external growth factors on the growth morphologies of

urea and β -succinic acid crystals. In order to further demonstrate the validity of the derived expression for growth, we are presently studying the growth morphology of several molecular and ionic crystals like different polymorphs of alanine, glycine, and KDP (KH_2PO_4) crystals from aqueous solutions. It is interesting to note that the solvents can also be used to obtain a desired polymorph of glycine crystals.⁶⁶ The discussed method can be extended to model the growth of different polymorph of glycine crystals in pure and mixed solvents. Our results clearly demonstrate that the growth expression derived in this manuscript will enable experimentalist to understand better the crystal growth process. It will provide them a better control over various parameters to obtain the desired crystal morphology. In view of this, we believe that the approach presented in this paper will aid in exploring the role played by solvent and different growth parameters on the kinetics and the shape of the molecular crystals from solutions.

■ ASSOCIATED CONTENT

Supporting Information

Detailed derivation of the growth rate expression and Figures 1–5. The lattice energy, optimized lattice parameters, and fractional coordinates of urea and β -succinic acid crystals calculated at different levels of theory, using various basis sets. This material is available free of charge via the Internet at <http://pubs.acs.org>.

■ AUTHOR INFORMATION

Corresponding Author

*E-mail: mksingh@rrcat.gov.in. Tel: +91-731-248-8677. Fax: +91-731-248-8650.

Notes

The authors declare no competing financial interest.

■ ACKNOWLEDGMENTS

The authors are grateful for the support and motivation received from Dr. P. K. Gupta. Discussions with S. K. Sharma and Prof. Julian Gale are gratefully acknowledged. The authors would like to thank Prof. Bartolomeo Civalleri for providing basis sets data. All the calculations were performed on Brahma and Nalanda Linux clusters at the computer centre, Raja Ramanna Centre for Advanced Technology.

■ REFERENCES

- (a) Bhushan, B.; Israelachvili, J. N.; Landman, U. *Nature* **1995**, 374, 607–616. (b) Johnson, E. *Science* **2002**, 296, 477–478. (c) Vlieg, E. *Surf. Sci.* **2002**, 500, 458–474.
- (a) Bourne, J. R.; Davey, R. J. *J. Cryst. Growth* **1976**, 36, 278–286. (b) Bourne, J. R.; Davey, R. J. *J. Cryst. Growth* **1976**, 36, 287–296.
- Bennema, P.; van Eerden, J. P. In *Morphology of Crystals*; Terra Scientific Publishing Company: Tokyo, 1977; pp 1–75.
- Shimon, L. J. W.; Vaida, M.; Addadi, L.; Lahav, M.; Leiserowitz, L. *J. Am. Chem. Soc.* **1990**, 112, 6215–6220.
- Bennema, P.; Gilmer, G. In *Crystal Growth: An Introduction*; Hartman, P., Ed.; North Holland: Amsterdam, 1973; pp 263–327.
- Simon, B.; Grassi, A.; Boistelle, R. *J. Cryst. Growth* **1974**, 26, 77–89.
- (a) Albon, N.; Dunning, W. J. *Acta Crystallogr.* **1962**, 15, 474–476. (b) Bennema, P. *J. Cryst. Growth* **1968**, 3–4, 331–334.
- Weissbuch, I.; Popovitz-Biro, R.; Lahav, M.; Leiserowitz, L. *Acta Crystallogr.* **1995**, B51, 115–148.
- Wells, A. F. *Discuss. Faraday Soc.* **1949**, 5, 197–201.
- Berkovitch-Yellin, Z. *J. Am. Chem. Soc.* **1985**, 107, 8239–8253.
- Davey, R. J.; Milisavljevic, B.; Bourne, J. R. *J. Phys. Chem.* **1988**, 92, 2032–2036.
- Weissbuch, I.; Shimon, L. J. W.; Landau, E. M.; Popovitz-Biro, R.; Berkovitch-Yellin, Z.; Addadi, L.; Lahav, M.; Leiserowitz, L. *Pure Appl. Chem.* **1986**, 58, 947–954.
- Weissbuch, I.; Addadi, L.; Lahav, M.; Leiserowitz, L. *Science* **1991**, 253, 637–645.
- Wang, J. L.; Leiserowitz, L.; Lahav, M. *J. Phys. Chem.* **1992**, 96, 15–16.
- Han, G.; Chow, P. S.; Tan, R. B. H. *Cryst. Growth Des.* **2011**, 11, 3941–3946.
- Chernov, A. A. *J. Cryst. Growth* **2004**, 264, 499–518.
- (a) Liu, X. Y.; Bennema, P. *Phys. Rev. B* **1996**, 53, 2314–2325. (b) Liu, X. Y.; Boek, E. S.; Briels, W. J.; Bennema, P. *Nature* **1995**, 374, 342–345. (c) Liu, X. Y.; Boek, E. S.; Briels, W. J.; Bennema, P. *J. Chem. Phys.* **1995**, 103, 3747–3754. (d) Liu, X. Y. *Phys. Rev. B* **1999**, 60, 2810–2817.
- Gnanasambandam, S.; Rajagopalan, R. *CrystEngComm* **2010**, 12, 1740–1749.
- (a) Bisker-Leib, V.; Doherty, M. F. *Cryst. Growth Des.* **2001**, 1, 455–461. (b) Lovette, M. A.; Doherty, M. F. *Cryst. Growth Des.* **2012**, 12, 656–669.
- Burton, W. K.; Cabrera, N.; Frank, F. C. *Philos. Trans. R. Soc. London* **1951**, A243, 299–357.
- (a) Piana, S.; Gale, J. D. *J. Am. Chem. Soc.* **2005**, 127, 1975–1982. (b) Piana, S.; Reyhani, M.; Gale, J. D. *Nature* **2005**, 438, 70–73.
- Davey, R.; Fila, W.; Garside, J. *J. Cryst. Growth* **1986**, 79, 607–613.
- Zeng, L.; Zha, M.; Ardoino, M.; Franzosi, P.; Zanotti, L.; Zuccalli, G.; Paorici, C. *J. Cryst. Growth* **1996**, 166, 528–532.
- Davey, R. J. *J. Cryst. Growth* **1986**, 76, 637–644.
- van der Voort, E. *J. Cryst. Growth* **1991**, 110, 662–668.
- Mullin, J. W.; Whiting, M. J. *L. Ind. Eng. Chem. Fundam.* **1980**, 19, 117–121.
- Doherty, R.; Roberts, K. J. *J. Cryst. Growth* **1988**, 88, 159–168.
- Davey, R. J.; Mullin, J. W.; Whiting, M. J. *J. Cryst. Growth* **1982**, 58, 304–312.
- Zhang, Y.; Doherty, M. F. *AIChE J.* **2004**, 50 (9), 2101–2112.
- Snyder, R. C.; Doherty, M. F. *AIChE J.* **2007**, 53 (5), 1337–1348.
- Ludlam-Brown, I.; York, P. *J. Phys. D: Appl. Phys.* **1993**, 26, B60–B65.
- (a) Singh, M. K.; Banerjee, A.; Gupta, P. K. *Cryst. Growth Des.* **2012**, 12, 732–741. (b) Singh, M. K.; Banerjee, A.; Gupta, P. K. *J. Cryst. Growth* **2012**, 343, 77–85.
- (a) Hartman, P.; Perdok, W. G. *Acta Crystallogr.* **1955**, 8, 49–52. (b) Hartman, P. In *Crystal Growth: An Introduction*; Hartman, P., Ed.; North Holland: Amsterdam, 1973; Chapter 14, pp 367–402.
- Jiang, X. N.; Xu, D. *J. Appl. Crystallogr.* **2003**, 36, 1448–1451.
- Chernov, A. A. *Contemp. Phys.* **1989**, 30, 251–276.
- (a) Rimer, J. D.; An, Z.; Zhu, Z.; Lee, M. H.; Goldfarb, D. S.; Wesson, J. A.; Ward, M. D. *Science* **2010**, 330, 337–341. (b) Vekilov, P. G.; Alexander, J. I. D. *Chem. Rev.* **2000**, 100, 2061–2090.
- Chernov, A. A. In *Modern Crystallography III*; Springer-Verlag: New York, 1984.
- Ohara, M.; Reid, R. C. In *Modelling Crystal Growth Rates from Solution*; Prentice Hall, Inc.: Upper Saddle River, NJ, 1973; pp 5–203.
- Cuppen, H. Theory and simulations of crystal growth - Fundamental steps in morphology prediction. Ph.D. Thesis, Radboud University, Nijmegen, The Netherlands, 2005.
- Reedijk, M. F.; Arsic, J.; Hollander, F. F. A.; de Vries, S. A.; Vlieg, E. *Phys. Rev. Lett.* **2003**, 90, 0661031–0661034.
- van der Eerden, J. P. In *Handbook of Crystal Growth*; Hurle, D. T. J., Ed.; Elsevier Science Publishers: Amsterdam, 1993; Vol. 1a, Chapter 5, pp 307–475.
- The adsorption of solvent molecules preferentially delays the growth of the faces and inhibits the rate of growth. Thus the growth rate should be inversely proportional to $E_{s-f}^{(hkl)}$.⁴⁰ On the other hand, growth rate is proportional to the concentration of solute molecules¹⁷

and inversely proportional to the concentration of solvent molecules. It should be noted that when $E_{s-f}^{(hkl)} \rightarrow \infty$ then $v_{\text{step}}^{(hkl)} \rightarrow 0$ and if $E_{s-f}^{(hkl)} \rightarrow 0$ then $v_{\text{step}}^{(hkl)} \propto \sigma$.⁴¹

(43) Fowler, S. R.; and Guggenheim, E. A. In *Statistical Thermodynamics*; Cambridge: London, 1960.

(44) The ordering of the solvent molecules at the interface can modify the interfacial structure in comparison to the interfacial structure from the vapor phase. When considering the effect of molecular orientation and relaxation induced by the solvent molecules at the surface, the product of slice energy and local dissolution enthalpy can be approximated by the product of the energy difference of isolated solute molecules in different orientations at the interface and in the bulk solutions ($E_{\text{molecule}}^{(hkl)}$)^{32a} and bulk dissolution enthalpy.

(45) Cardew, P. T.; Davey, R. J.; Garside, J. *J. Cryst. Growth* **1979**, *46*, 534–538.

(46) Singh, M. K.; Banerjee, A. *Cryst. Res. Technol.* **2011**, *46*, 1035–1043.

(47) Singh, M. K.; Banerjee, A. Manuscript in preparation.

(48) Dovesi, R.; Saunders, V. R.; Roetti, C.; Orlando, R.; Zicovich-Wilson, C. M.; Pascale, F.; Civalleri, B.; Doll, K.; Harrison, N. M.; Bush, I. J.; D'Arco, P.; and Llunell, M. *CRYSTAL09 (CRYSTAL09 User's Manual)*; University of Torino: Torino, 2009.

(49) Grimme, S. *J. Comput. Chem.* **2006**, *27*, 1787–1799.

(50) (a) Civalleri, B.; Zicovich-Wilson, C. M.; Valenzano, L.; Ugliengo, P. *CrystEngComm* **2008**, *10*, 405–410. (b) Civalleri, B.; Doll, K.; Zicovich-Wilson, C. M. *J. Phys. Chem. B* **2007**, *111*, 26–33.

(51) Singh, M. K.; Banerjee, A. *CrystEngComm* **2013**, *15*, 4143–4152.

(52) Hehre, W. J.; Radom, L.; Schleyer, P. v. R.; Pople, J. A. In *Ab Initio Molecular Orbital Theory*; Wiley: New York, 1986.

(53) (a) Gilat, G. *J. Comput. Phys.* **1972**, *10*, 432–465.

(b) Monkhorst, H. J.; Pack, J. D. *Phys. Rev. B* **1976**, *13*, 5188–5192.

(54) (a) Doll, K.; Saunders, V. R.; Harrison, N. M. *Int. J. Quantum Chem.* **2001**, *82*, 1–13. (b) Doll, K.; Dovesi, R.; Orlando, R. *Theor. Chem. Acc.* **2004**, *112*, 394–402.

(55) (a) Feng, S.; Li, T. *J. Chem. Theory Comput.* **2006**, *2*, 149–156.

(b) Dobson, J. F.; McLennan, K.; Rubio, A.; Wang, J.; Gould, T.; Le, H. M.; Dinte, B. P. *Aust. J. Chem.* **2001**, *54*, 513–527.

(56) Schaftenaar, G.; Noordik, J. H. *J. Comput.-Aided Mol. Des.* **2000**, *14*, 123–134.

(57) Boek, E. S.; Briels, W. J.; van Eerden, J.; Feil, D. *J. Chem. Phys.* **1992**, *96*, 7010–7018.

(58) Gavezzotti, A. *Modell. Simul. Mater. Sci. Eng.* **2002**, *10*, R1–R29.

(59) (a) Rae, A. I. M.; Mason, R. *Proc. R. Soc. London, Ser. A* **1968**, *304*, 487–499. (b) Gilli, G. In *Molecule and Molecular Crystals; Fundamental of Crystallography*; Giacovazzo, C., Ed.; Oxford University Press: NY, 2011; Chapter 8.

(60) Swaminathan, S.; Craven, B. M.; McMullan, R. K. *Acta Crystallogr.* **1984**, *B40*, 300–306.

(61) Broadley, J. S.; Cruickshank, D. W. J.; Morrison, J. D.; Robertson, J. M.; Shearer, H. M. M. *Proc. R. Soc. London, Ser. A* **1959**, *251* (No. 1267), 441–457.

(62) (a) Ferro, D.; Barone, G.; Della Gatta, G.; Piacente, V. *J. Chem. Thermodyn.* **1987**, *19*, 915–923. (b) Cox, J. D.; Pilcher, G. In *Thermochemistry of Organic and Organometallic Compounds*; Academic Press: London, 1970.

(63) Momany, F. A.; Carruthers, L. M.; McGuire, R. F.; Scheraga, H. A. *J. Phys. Chem.* **1974**, *78*, 1595–1620.

(64) Maschio, L.; Usyat, D.; Civalleri, B. *CrystEngComm* **2010**, *12*, 2429–2435.

(65) The energy correction is required because in liquid water, each water molecule is associated with 4 hydrogen bonds (H bond). The average energy of a fully formed icelike structure is of –23.0 kJ/mol. Due to the bonding of water molecules with the urea molecules at the surface, only one H bond is altered and the remaining three are unchanged. The energy needed to make this new binding is the difference between calculated $E_{s-f}^{(hkl)}$ and –5.8 kJ/mol. Similarly, in liquid methanol, each methanol molecule is associated with 2 H bonds. The bonding of the methanol molecule to the crystal surfaces, only one H bond is altered and the remaining one is unchanged. Thus,

energy needed to make a new bond is the difference between calculated $E_{s-f}^{(hkl)}$ and –10.9 kJ/mol.

(66) Weissbuch, I.; Torbeev, V. Yu.; Leiserowitz, L.; Lahav, M. *Angew. Chem.* **2005**, *117*, 3290–3293.